Large-amplitude Q_n-Q_p collectivity in the neutron-rich oxygen isotope ^{20}O

A. P. Severyukhin,[1] M. Bender,[2,3] H. Flocard,[4] and P.-H. Heenen[5]

[1] *Bogoliubov Laboratory of Theoretical Physics, Joint Institute for Nuclear Research, 141980 Dubna, Moscow region, Russia*
[2] *Dapnia/SPhN, CEA Saclay, F-91191 Gif sur Yvette Cedex, France*
[3] *Université Bordeaux 1; CNRS/IN2P3; Centre d'Etudes Nucléaires de Bordeaux Gradignan, UMR5797, Chemin du Solarium, BP120, F-33175 Gradignan, France*
[4] *CNRS-IN2P3, Université Paris XI, CSNSM, Bt. 104, F-91405 Orsay Campus, France*
[5] *PNTPM, CP229, Université Libre de Bruxelles, B-1050 Brussels, Belgium*

(Dated: January 12 2007)

By means of HFB calculations with independent constraints on axial neutron and proton quadrupole moments $\hat{Q}_n$ and $\hat{Q}_p$, we investigate the large amplitude isoscalar and isovector deformation properties of the neutron-rich isotope ^{20}O. Using the particle-number and angular-momentum projected Generator Coordinate Method, we analyze the collective dynamics in the $\{\langle\hat{Q}_n\rangle, \langle\hat{Q}_p\rangle\}$ plane. The parameterization SLy4 of the Skyrme interaction is used for all calculations in connection with a density-dependent zero-range pairing interaction. Our results show that already for this moderately neutron-rich nucleus the transition moments are modified when independent neutron and proton collective dynamics are allowed.

PACS numbers: 21.60.Jz, 21.10.Gv, 21.10.Ky, 27.30.+t

I. INTRODUCTION

The dominance of the neutron-proton attraction is one of the main characteristics of the effective nucleon-nucleon interaction. It can be traced back to the isospin symmetry of the force and to the cooperation of the $T = 0$ and $T = 1$ channels. As a result, isovector collective modes have a much higher excitation energy than their isoscalar counterparts. On the other hand, the study of nuclei away from the stability line has led to the discovery of phenomena (halo and molecular nuclei, reorganization of the shell structure) which challenge some of the standard nuclear structure concepts. These new perspectives have been mostly provided by the analysis of neutron-rich nuclei which, because of the relative weakening of Coulomb effects, give the best opportunities to investigate dynamics far away from the $N = Z$ line. The new phenomena are partly attributed to a decoupling of the two nucleonic distributions when N exceeds Z by far. Another cause invoked is the weak binding of the last occupied neutrons in the absence of a barrier. Aside from new features of ground-state properties, also some interesting effects, such as pigmy resonances, have been observed which are clear indications that the excitation of isovector modes is easier in neutron-rich isotopes than in stable nuclei. The pigmy modes are associated with dipolar excitations involving a restricted number of nucleons and partly for this reason, carrying a small fraction of the sum rule only. They also correspond to collective vibrations. On the other hand, most of the low-energy collective structure remains dominated by isoscalar large amplitude quadrupole dynamics, leading in many regions of the nuclear chart to ground state deformations.

The strong proton shell closure at $Z = 8$ and the already good experimental knowledge of the complete oxygen isotope series from ^{16}O up to the drip line at ^{24}O [1, 2, 3, 4, 5, 6, 7, 8, 9, 10, 11, 12, 13, 14, 15, 16, 17, 18] makes Oxygen an attractive element for a first investigation (not to mention that the theoretical analysis is significantly simplified in light systems). In fact, the experimental effort on these isotopes has spurred a number of analysis based either on the mean-field method [13, 19, 20, 21, 22, 23, 24] or on the shell model [18, 25, 26, 27]. Mean-field investigations of collective dynamics properties have up to now exclusively concerned excitations about the lowest configuration which always correspond to zero mass quadrupole moment. An important result from both experimental and theoretical works is the weakening of the $N = 20$ shell effect (both ^{26}O and ^{28}O are not bound [3, 4, 5, 6]) along with evidences for a local subshell predicted sometimes at $N = 14$ [13] or at $N = 16$ [23].

For these reasons, we have chosen to investigate in a consistent way the effect of large neutron excess on both isoscalar and isovector quadrupole modes of the oxygen isotopes. This first article presents our method and gives an illustration for the nucleus ^{20}O. In order to treat small- and large-amplitude collective motion on the same footing, we perform our analysis within the framework of the projected generator coordinate method (GCM) [28, 29, 30] based on Hartree-Fock-Bogoliubov (HFB) wave functions. A consistent simultaneous treatment of isovector and isoscalar dynamics is attempted by working in a GCM collective space in which neutron and proton deformations are allowed to vary independently.

II. DEFINITION OF THE COLLECTIVE SPACE

Let us briefly summarize the different steps involved in the projected configuration mixing calculation (see Refs. [28, 29, 30] for more details).

In the GCM, the collective dynamics is constrained by the choice of a variational space, the so-called collective

space. For the present study, this space is generated by a non-orthogonal basis of particle-number and angular-momentum projected HFB states.

A. Constrained HFB

The HFB states are obtained from self-consistent calculations using either a single constraint on the axial mass quadrupole moment, or a double constraint acting separately on the axial neutron and proton quadrupole moments. The resulting HFB states are denoted $|q\rangle$, where q labels the collective variables. In the case of a single constraint, q is identified with the expectation value $\langle\hat{Q}\rangle$. The dynamics will be studied along only one collective dimension, the total deformation. The relative contributions of $\langle\hat{Q}_n\rangle$ and $\langle\hat{Q}_p\rangle$ to the total quadrupole moment $\langle\hat{Q}_t\rangle$ are then entirely determined by the CHFB minimization process. In the case of double contraint, the proton $\langle\hat{Q}_p\rangle$ and neutron $\langle\hat{Q}_n\rangle$ quadrupole moments are taken as independent constraints, and the collective variable q becomes two-dimensional, $q = \{\langle\hat{Q}_n\rangle, \langle\hat{Q}_p\rangle\}$.

As in our previous studies [28, 29, 30], the Lipkin-Nogami (LN) prescription is used to avoid a spurious collapse of pairing correlations in the HFB wave functions for all values of the quadrupole moment. The HFB-LN equations are solved with the two-basis method described in Ref. [31]. The HFB states are chosen to be time-reversal invariant, and the single-particle states are eigenstates of parity, z signature, and projection of isospin as in Ref. [32]. They are represented on 1/8 of a cubic mesh of size 11.6 fm with a distance of 0.8 fm between mesh points.

We use the effective Skyrme interaction SLy4 in the particle-hole channel [33] together with a surface-peaked density-dependent zero-range force acting in the particle-particle (pairing) channel. Its strength is taken equal to -1000 MeV fm^3 in connection with two soft cutoffs at 5 MeV above and below the Fermi energies as introduced in Ref. [34].

As a matter of fact, the one-body potentials associated with the standard axial quadrupole operator

$$\hat{Q} = 2\hat{z}^2 - \hat{x}^2 - \hat{y}^2 \tag{1}$$

have a numerically pathological behavior at large distances. Indeed, depending on whether the deformation is prolate or oblate, the constraining field decreases as $-r^2$ along the z axis or in the perpendicular plane, respectively. When solving the mean-field equations on a mesh in coordinate space, the finite size of the mesh cuts the constraint at large distances, but there always remain attractive pockets at the boundaries of the box, which will either distort the single-particle states around the continuum threshold, or even bind them. [1] As soon as these states have a sizable occupation, as it happens in neutron-rich systems, this will often lead to spurious results. The large box sizes that have to be chosen in neutron-rich systems as discussed here even amplify the problem; hence, the constraint has to be damped at large distances from the nucleus. We achieve this by multiplying the constraining operator with a Fermi function as proposed in Ref. [36]. We first define an equidensity surface on which the nucleon density ρ is equal to one tenth of the maximal density $\rho_{\max}$. The cutoff takes place smoothly over a width equal to a for radii exceeding the surface by a distance δr_c.

The parameters δr_c and a have to be selected such that they do not affect the results over the range of considered deformations. The main role is played by the cutoff distance δr_c which we have set to 5.5 fm, slightly larger than the recommended value of Ref. [36], while the width parameter was set to $a = 0.4$ fm.

B. Particle-number and angular-momentum projected GCM

The second step of our method is the construction of the collective basis

$$|JMq\rangle = \frac{1}{\mathcal{N}}\,\hat{P}^J_{M0}\,\hat{P}^N\,\hat{P}^Z\,|q\rangle, \tag{2}$$

by means of projection operators, where $\mathcal{N} = \langle q|\hat{P}^J_{00}\,\hat{P}^N\,\hat{P}^Z\,|q\rangle^{1/2}$ is a normalization factor. Although the particle numbers of the intrinsic and projected states might be chosen different, we do not make use of this freedom and use $N = 12$ and $Z = 8$ everywhere, and drop the particle number indices for the sake of simple notation.

The projection operator $\hat{P}^J_{MK}$ restores the rotational invariance broken by the intrinsic deformation of the nucleus and provides a state with the good total angular momentum J. As we consider only axial deformations with the z axis as symmetry axis, the projection of the third angular momentum component K in the intrinsic frame is equal to zero by construction. We limit our study to values of the total angular momentum J equal to zero and two.

In the next stage, we construct collective wave functions from a linear combination of projected states

$$|JMk\rangle = \sum_q f^J_{kq}|JMq\rangle. \tag{3}$$

The weights $f^J_{k,q}$ of the projected HFB states are determined from the minimization of the total energy

$$E^J_k = \frac{\langle JMk|\hat{H}|JMk\rangle}{\langle JMk|JMk\rangle}. \tag{4}$$

[1] When the CHFB calculations are performed by expanding single-particle orbitals on a basis such as an oscillator basis, the effective cutoff is provided by the long-range behavior of the basis wave functions.

The index k has been introduced to label the several solutions of the minimization equation which we will assign to the GCM ground state and to excited states for each angular momentum J. The variation of the energy ($\delta_f E_k^J = 0$) leads to the Hill-Wheeler-Griffin equation

$$\sum_{q'} \left(\mathcal{H}^J_{qq'} - E^J_k \, \mathcal{I}^J_{qq'} \right) f^J_{kq'} = 0. \tag{5}$$

Its solution requires to compute the off-diagonal matrix elements of the energy and overlap kernels

$$\mathcal{H}^J_{qq'} = \langle JMq|\hat{H}|JMq'\rangle \tag{6}$$
$$\mathcal{I}^J_{qq'} = \langle JMq|JMq'\rangle, \tag{7}$$

which are evaluated with the techniques described in [28]. The calculation of electromagnetic transition of order L requires an additional evaluation of the projected GCM kernels associated with the electric and magnetic tensor operators $\hat{T}^{[L,M=0]}$:

$$\mathcal{T}^{J,[L,0]J'}_{qq'} = \langle JMq|\hat{T}^{[L,0]}|J'M'q'\rangle, \tag{8}$$

where J, L and J' satisfy the triangle inequalities.

Two comments are in order. First, aside from restoring the symmetries broken at the mean-field level, the projection also performs a transformation from the intrinsic to the laboratory frame. As a consequence, every state $|J=0\,M=0\,q\rangle$ is *spherical* in the laboratory frame of reference irrespective of the intrinsic quadrupole deformation associated with the collective variable q. Second, the coefficients f^J_{kq} are directly connected to the collective wave-function g^J_{kq} which provide informations on the spreading of this wave function over the collective space spanned by the variable(s) q. A set of orthogonal collective wave functions g^J_{kq} is given by [37]

$$g^J_{kq} = \sum_{q'} (\mathcal{I}^J)^{1/2}_{qq'} \, f^J_{kq}, \tag{9}$$

where $(\mathcal{I}^J)^{1/2}$ represents the kernel whose square convolution gives $\mathcal{I}^{\mathcal{J}}$.

Numerically speaking, the GCM calculations are quite demanding. Given the number of grid points selected on the $\{\langle\hat{Q}_n\rangle, \langle\hat{Q}_p\rangle\}$ surface (about 25), the number of gauge angles to restore the particle numbers (7 for both protons and neutrons) and the number of Euler required for an accurate angular-momentum projection (12), each calculation corresponds to the mixing of about 15 thousand N-body wave functions. An additional difficulty is related the non-orthogonality of the GCM basis that generates near-zero eigenvalues of the overlap kernel $\mathcal{I}_{qq'}$, which might lead to spurious states. These difficulties are treated with techniques described in Refs. [28, 29, 30].

III. RESULTS

In the left panel of Fig. 1, we show the CHFB energy curve obtained with a single constraint on the mass quadrupole deformation as a function of the dimensionless quadrupole deformation $\beta_{2,t}$

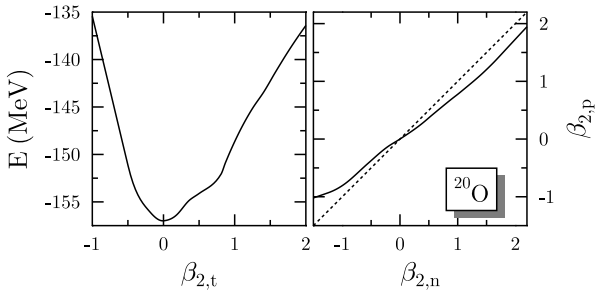

FIG. 1: Particle-number projected energy curve obtained with a single constraint on the mass quadrupole moment (left) and the corresponding path in the plane of proton and neutron quadrupole deformation (right). The dotted line in the right panel corresponds to the line of equal proton and neutron deformation $\beta_{2,n} = \beta_{2,p}$.

$$\beta_{2,t} = \sqrt{\frac{5}{16\pi}} \, \frac{4\pi \, Q_t}{3R^2A} \tag{10}$$

where the radius constant is given by $R = 1.2\ A^{1/3}$ fm. Please note that in light nuclei and at large deformation; the values of the β_2 as defined through Eq. 10 might be much larger than the generating multipole deformation in a liquid drop model. Please note also that, as in our previous works, the mean-field energy curves that are presented are already particle-number projected, to avoid the ambiguities related to the Lipkin-Nogami correction to the mean-field energy. In the right panel of Fig. 1, we show the path followed by the single contraint results in the two-dimensional plane of proton and neutron deformations

$$\beta_{2,n} = \sqrt{\frac{5}{16\pi}} \, \frac{4\pi \, Q_n}{3R^2N} \tag{11a}$$
$$\beta_{2,p} = \sqrt{\frac{5}{16\pi}} \, \frac{4\pi \, Q_p}{3R^2Z}. \tag{11b}$$

This path corresponds to the valley that is obtained in a double-contraint calculation. Please note that, as long as the radii of the proton and neutron density distributions are not too different, the use of $\beta_{2,n}$ and $\beta_{2,p}$ removes most of the trivial scaling of the neutron and proton quadrupole moments associated with different values of N and Z. With such coordinates, equal neutron and proton deformation of a saturating system where the neutron density is strictly proportional to the proton density would lie on the first bisector, represented by the dotted line in the right panel of Fig. 1. Already for not too large deformations, the path diverts substantially from the line of equal proton and neutron deformations, indicating that for both prolate and oblate shapes the neutrons are more deformed than the protons.

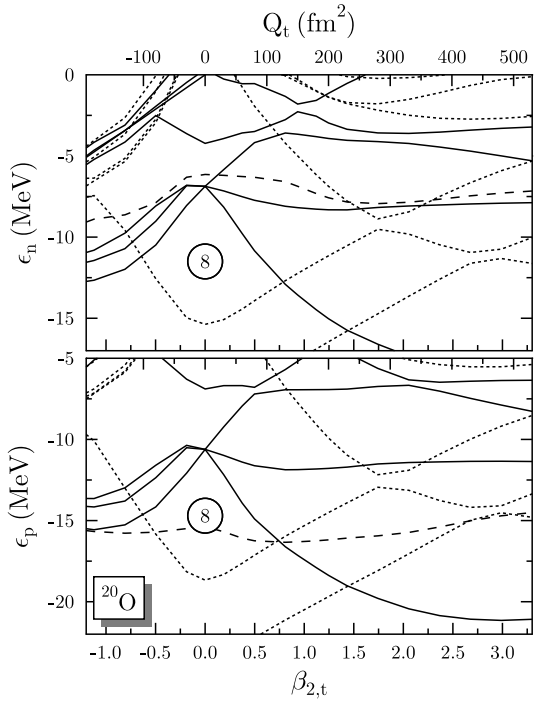

FIG. 2: Neutron (top) and proton (bottom) single-particle energies (in MeV) versus mass quadrupole deformation (bottom horizontal scales) and mass quadrupole moment (top horizontal scale). Solid (dotted) lines correspond to positive (negative) parity states. The dashed lines represent the Fermi energies of protons and neutrons, respectively.

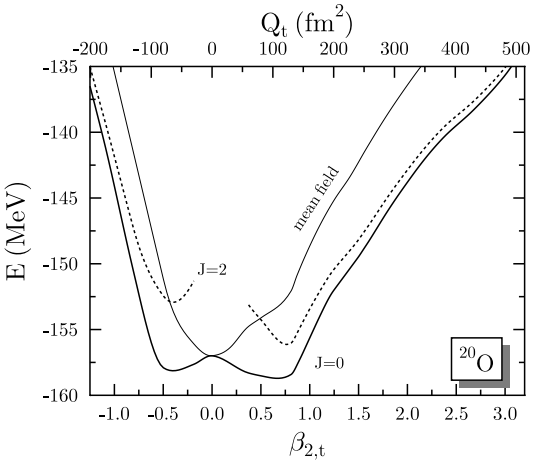

FIG. 3: Particle-number projected mean-field (solid curve) and particle-number and angular-momentum projected deformation energy curves of ^{20}O as a function of the mass quadrupole deformation.

The Nilsson diagrams of neutron and proton single-particle energies as obtained with SLy4 for ^{20}O are shown in Fig. 2 along the path of Fig. 1. Qualitatively, both are very similar. For neutrons, however, the upward shift of the Fermi energy leads to a particle-hole (ph) excitation at $\beta_{2,t} \approx 1.8$ ($\langle\hat{Q}_t\rangle \approx 300$ fm^2) in which the $\nu\ p_{1/2}$ level is exchanged with the $\nu\ f_{7/2}\ m = 1/2$ level. The sequence of crossings at the Fermi surface for the protons corresponds to a 2p-2h ($\beta \approx 0.6$) and 4p-4h proton excitation ($\beta \approx 3$) and is close to that obtained for ^{16}O in Ref. [35].

In Fig. 3 are drawn the deformation energy curves corresponding to three different calculations. The number-projected HFB energies are represented by a thin solid curve. It displays a pattern typical for an oxygen isotope: a well-defined spherical minimum and a steep rise of the energy versus deformation, with a shoulder hinted at moderate proton deformation. For the energy curve projected on $J = 0$, the behavior is markedly different. The energy does not vary much over the range $-0.5 < \beta_{2,t} < 0.8$, or -100 fm^2 $< \langle\hat{Q}_t\rangle < 200$ fm^2, equivalently. This reflects that the 0p-0h configuration with respect to the spherical HFB solution is the dominant component of the $J = 0$ wave function and that this component is present in the mean-field wave function over a rather large range of deformations. The part of the curve beyond $\beta_{2,t} \simeq 0.8$, or $\langle\hat{Q}_t\rangle \simeq 120$ fm^2, respectively, corresponds to the transition associated with a 2p-2h proton excitation across the magic gap at $Z = 8$. These features have been studied in detail in Ref. [35] for ^{16}O. In particular, it has been shown to explain successfully the very low excitation energy of the first excited 0^+ state of this isotope. By contrast, the 2^+ energy curve displays marked minima. The fact that for almost all deformations but those close to sphericity the number-projected CHFB curve lies significantly above the 0^+ and 2^+ curves shows that components of higher angular momentum have a non-negligible amplitude in the intrinsic HFB states $|q\rangle$.

In the rest of this work, we consider only neutron and proton deformations such that the HFB excitation energy does not exceed 20 MeV. The associated zone in the $\{\langle\hat{Q}_n\rangle, \langle\hat{Q}_p\rangle\}$ plane corresponds to configurations in which the proton $1s_{1/2^+}$ and $1p_{3/2^-}$ orbitals remain filled.

In Fig. 4 are shown the $J = 0$ (top) and $J = 2$ (bottom) projected energy surfaces. The $J = 0$ surface displays two minima, in the quadrants where both neutrons and protons have either prolate or oblate deformations. One notes that the energy rises slowly along the axis $\langle\hat{Q}_n\rangle = 0$ in contrast with the single constraint CHFB path indicated by the dash line. A similar, although less marked tendency exists along the $\langle\hat{Q}_p\rangle = 0$ axis. This indicates that the 0^+ component in the intrinsic HFB state is mostly unchanged along these axes and also that there already exists a relative decoupling of proton and neutron deformations in this neutron-rich oxygen isotope.

Figure 5 displays the collective GCM wave functions g^J_{kq}, Eq. (9), for the lowest $J = 0$ and $J = 2$ states obtained when restricting the collective motion to the one-dimensional path given by the dotted line in Fig. 4. On the one hand, the $J = 0$ ground-state wave function is localized in the vicinity of $\langle\hat{Q}_t\rangle = 0$, as expected from the potential energy surface. On the other hand, it displays an asymmetry favoring prolate deformations.

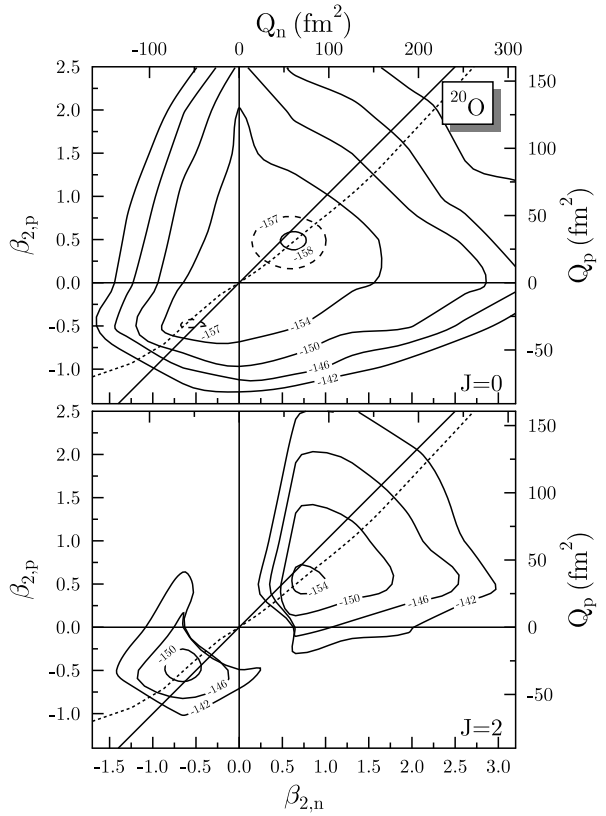

FIG. 4: Contour lines of the angular-momentum and particle-particle number projected deformation energy surface of ^{20}O (in MeV) as a function of the neutron and proton deformation $\beta_{2,\tau}$, $\tau = n, p$. The right and upper axes show the corresponding proton and neutron quadrupole moments Q_τ, $\tau = n, p$. The upper panel shows the surface for $J = 0$, the lower panel for $J = 2$. The solid line in both panels represents the line of equal proton and neutron deformation $\beta_{2,p} = \beta_{2,n}$, the dotted line the isoscalar path followed when a single constraint on the mass quadrupole moment $\hat{Q}_t$ is applied.

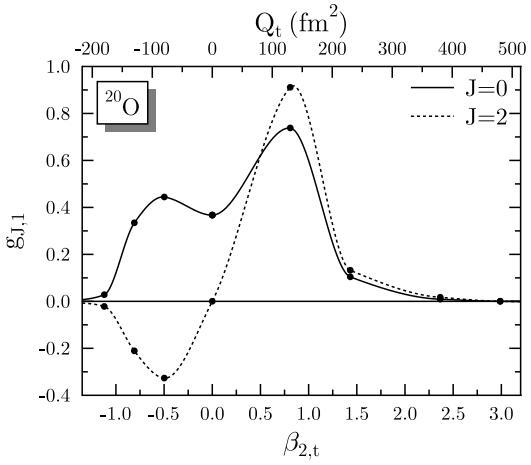

FIG. 5: GCM wave functions of the 0^+ ground state and the lowest $J = 2$ state of ^{20}O for a collective motion restricted to one dimension, plotted versus the mass quadrupole deformation $\beta_{2,t}$.

The representation of the two-dimensional wave function is complicated by the fact that the discretized GCM wave function, Eq. (3), is defined without a volume element. As a consequence, the value of the collective wave function g^J_{kq} at a given point q represents the wave function times an unspecified volume element, that depends on the distribution of the surrounding points. On the one hand, this definition of the GCM wave function allows to optimize the set of basis states and to remove redundant states without any difficulty. On the other hand, any attempt to plot a GCM wave function built from unevenly distributed points might be very misleading as any curve used to interpolate these points to guide the eye is, strictly speaking, meaningless. A plot of a one-dimensional wave function g^J_{kq}, as given in Fig. 5, is of course also affected, but in one dimension one can almost always achieve a distribution of basis states that still allows an intuitive interpretation of the collective wave function. There are further issues, as the only proper metric is defined by the overlap kernels, not the generator coordinates, which furthermore are different for each angular momentum. These points, which affect merely the presentation and interpretation of a GCM wave function, but not its physical content, deserve further attention in the future. Anyway, for the multi-dimensional wave function of ^{20}O the points that can be chosen without having redundant ones in the basis of projected HFB states have to be irregularly distributed indeed.[2] As there is no unambiguous way to plot a two-dimensional wave function for the distribution of basis states we have used here, we will not attempt to do so, but restrict the further discussion to the observables calculated from it. However, we can state that when adding states with a different proton-to-neutron ratio of the deformation to one-dimensional path from the constraint on the mass quadrupole moment, the dominating contribution to the lowest $J = 0$ and $J = 2$ GCM states always remains the state with $\beta_2 \approx 0.8$ located on the one-dimensional path.

The 2^+ energy surface (bottom part of Fig. 4) is split into two wells in the fully prolate and oblate sectors (upper right and lower left quadrants). In the prolate sector the energy surface is markedly deeper. This is a good indication that the collective dynamics will favor a prolate deformation of the first 2^+ state. The minimum on this surface is shifted to the region where the neutron deformation is larger than the proton deformation. This agrees with QRPA calculations [21], as well as with experimental evidences [20]. The properties of the first 2^+ level are summarized in Table I.

In an attempt to systematically add states that cover the whole β_n-β_p plane to the one-dimensional calcula-

[2] There are in fact several near-equivalent sets which have a very different distribution in the $\langle\hat{Q}_n\rangle$, $\langle\hat{Q}_p\rangle$ plane.

deformation space	E (MeV)	$B(E2\uparrow)$ (e^2 fm^4)
$\{\langle\hat{Q}_t\rangle\}$	3.1±0.1	80±10
$\{\langle\hat{Q}_n\rangle, \langle\hat{Q}_p\rangle\}$	3.2±0.2	180±50
Experiment	1.7	28± 2

TABLE I: Properties of the lowest calculated 2^+ state in ^{20}O for the two choices of the deformation space considered here in comparison with experimental data taken from Ref. [1].

tion depicted in Fig. 5, it turns out that the GCM basis becomes quickly highly redundant, which is reflected by the presence of several small eigenvalues of the norm kernel. To avoid spurious states which would lead to large numerical inaccuracies on energies and transition probabilities, one must avoid a very dense and regular two-dimensional mesh. This problem is particularly pronounced in a light nucleus as ^{20}O, in which a SCMF wave function changes very slowly with deformation, but becomes more marginal for nuclei beyond the *sd* shell. Therefore, one has to make several calculations with different choices for the set of SCMF states, and use the variational principle to select the mesh giving the lowest energies without giving rise to spurious contributions. The uncertainty given in Table I is a measure of the fluctuations of the results when using a different set of points in the $\{\langle\hat{Q}_n\rangle, \langle\hat{Q}_p\rangle\}$ space before entering a zone of numerical instability. It is noteworthy that the $B(E2)$ value (and its equivalent for the neutron density distribution) fluctuate much more in dependence of the chosen set of SCMF states than the total energies of the first 0^+ and 2^+ states.

The energy gain from the full isospin dynamics is of about 800 keV for both the ground state and the lowest 2^+ state, leaving the excitation of the 2^+ state nearly unchanged. The experimental value is overestimated by 1.4 MeV. This discrepancy is in the range of values observed in a global study of the properties of the first 2^+ states in even-even nuclei [38], performed with a method similar to the one used. The possible origins of this discrepancy are also discussed in Ref. [38], and for ^{20}O, they are presumably twofold. The variational calculation would be improved for the lowest 2^+ state if it was constructed from a $J_z = 2$ cranked constrained set of wave functions rather than from $J_z = 0$ set as is done here. There is also a lack of broken-pair two-quasiparticle components breaking time reversal invariance in the variational space, which should play a role in this semi-magic nucleus, see the discussion of chains of heavier semi-magic nuclei in Ref. [38].

In disagreement with the global trend found by Sabbey *et al.* [38], the $B(E2)$ value is in much worse agreement with the data than the excitation energy. The effect of a larger variational space from a double constraint is even going in the wrong direction, leading to an overestimation of the $B(E2)$ value by a factor 6. The value of the ratio between neutron and proton transition matrix elements is $M_n/M_p \approx 2.1 > N/Z$. This is less than the experimental or the QRPA values calculated with the same force [21]. It indicates that the protons follow too closely the neutrons when deforming the nucleus, which leads to the too large $B(E2)$ value that we obtain. Since the QRPA value for the $B(E2)$ obtained with the same effective interaction is much larger,[3] this probably points out to a deficiency of our variational space rather than to a problem due to the effective interaction. The presence of broken-pair two-quasiparticle states breaking time-reversal invariance in the 2^+ wave function could reduce the $B(E2)$ value and go into the right direction, but the present stage of our method does not allow to test the magnitude of this effect.

IV. CONCLUSIONS

We have started an investigation of the large-amplitude quadrupole dynamics in neutron-rich nuclei taking into account the full isospin space. Among our initial motivation was the search for stable configurations in which neutron and proton display different static deformation. Our results indicate that it is indeed the case when the usual dimensionless deformations $\beta_{2,n}$ and $\beta_{2,p}$ are used to remove the trivial scaling of the quadrupole moments with neutron and proton number.

We have also looked for signs of a dynamical isospin instability which would show up in specific spectroscopic properties. At a qualitative level, we observe the importance of allowing independent proton and neutron deformation: although the main features of the collective wave functions are still the same as those determined by the one-dimensional dynamics, the full wave function displays a significant extension on both sides of this path. Similarly, there is a clear influence on the transition moments. Unfortunately, the agreement with the experimental data is not satisfactory for this light nucleus. Our model would probably be improved by enlarging the variational space for the 2^+ state with the inclusion of states breaking time-reversal invariance. The developments which will allow this inclusion are still underway.

Acknowledgments

Part of the work by M. B. was performed within the framework of L'Espace de Structure Nucléaire Théorique (ESNT). This work has been partly supported by the PAI P5-07 of the Belgian Science Policy Office.

[3] It has to be noted that the QRPA calculations of Ref. [21] make simplifying approximations for the residual interaction, which have unclear consequences for the observables discussed here.

[1] S. Raman, C. H. Malarkey, W. T. Milner, C. W. Nestor, Jr. and P. H. Stelson, At. Data Nucl. Data Tables **36**, 1 (1987).

[2] J. L. Escudié, R. Lombard, M. Pignanelli, F. Resmini, and A. Tarrats, Phys. Rev. C **10**, 1645 (1974); Phys. Rev. C **11**, 639(E) (1975).

[3] O. Tarasov, R. Allatt, J. C. Anglique, R. Anne, C. Borcea, Z. Dlouhy, C. Donzaud, S. Grévy, D. Guillemaud-Mueller, M. Lewitowicz, S. Lukyanov, A. C. Mueller, F. Nowacki, Yu. Oganessian, N. A. Orr, A. N. Ostrowski, R. D. Page, Yu. Penionzhkevich, F. Pougheon, A. Reed, M. G. Saint-Laurent, W. Schwab, E. Sokol, O. Sorlin, W. Trinder and J. S. Winfield, Phys. Lett. **B409**, 64 (1997).

[4] H. Sakurai, S. M. Lukyanov, M. Notani, N. Aoi, D. Beaumel, N. Fukuda, M. Hirai, E. Ideguchi, N. Imai, M. Ishihara, H. Iwasaki, T. Kubo, K. Kusaka, H. Kumagai, T. Nakamura, H. Ogawa, Yu. E. Penionzhkevich, T. Teranishi, Y. X. Watanabe, K. Yoneda and A. Yoshida, Phys. Lett. **B448**, 180 (1999).

[5] A. Ozawa, O. Bochkarev, L. Chulkov, D. Cortina, H. Geissel, M. Hellström, M. Ivanov, R. Janik, K. Kimura, T. Kobayashi, A. A. Korsheninnikov, G. Münzenberg, F. Nickel, A. A. Ogloblin, M. Pfützner, V. Pribora, H. Simon, B. Sitárd, P. Strmen, K. Sümmerer, T. Suzuki, I. Tanihata, M. Winkler and K. Yoshida, Nucl. Phys. **A673**, 411 (2000).

[6] M. Thoennessen, T. Baumann, J. Enders, N. H. Frank, P. Heckman, J. P. Seitz, A. Stolz and E. Tryggestad, Nucl. Phys. **A722**, 61c (2003).

[7] M. Thoennessen, T. Baumann, B. A. Brown, J. Enders, N. Frank, P. G. Hansen, P. Heckman, B. A. Luther, J. Seitz, A. Stolz, and E. Tryggestad, Phys. Rev. C **68**, 044318 (2003).

[8] M. Belleguic, M.-J. Lòpez-Jiménez, M. Stanoiu, F. Azaiez, M.-G. Saint-Laurent, O. Sorlin, N. L. Achouri, J. -C. Angélique, C. Bourgeois, C. Borcea, J. -M. Daugas, C. Donzaud, F. De Oliveira-Santos, J. Duprat, S. Grévy, D. Guillemaud-Mueller, S. Leenhardt, M. Lewitowicz, Yu.-E. Penionzhkevich and Yu. Sobolev, Nucl. Phys. **A682**, 136c (2001).

[9] Y. Blumenfeld, Nucl. Phys. **A752**, 279c (2005).

[10] J. K. Jewel, L. A. Riley, P. D. Cottle, K. W. Kemper, T. Glasmacher, R. W. Ibbotson, H. Scheit, M. Chromik, Y. Blumenfeld, S. E. Hirzebruch, F. Maréchal and T. Suomijärvi, Phys. Lett. **B454**, 181 (1999).

[11] P. G. Thirolf, B. V. Pritychenko, B. A. Brown, P. D. Cottle, M. Chromik, T. Glasmacher, G. Hackman, R. W. Ibbotson, K. W. Kemper, T. Otsuka, L. A. Riley and H. Scheit, Phys. Lett. **B485**, 16 (2000).

[12] M. Stanoiu, F. Azaiez, Zs. Dombrádi, O. Sorlin, B. A. Brown, M. Belleguic, D. Sohler, M. G. Saint Laurent, M. J. Lopez-Jimenez, Y. E. Penionzhkevich, G. Sletten, N. L. Achouri, J. C. Angélique, F. Becker, C. Borcea, C. Bourgeois, A. Bracco, J. M. Daugas, Z. Dlouhý, C. Donzaud, J. Duprat, Zs. Fülöp, D. Guillemaud-Mueller, S. Grévy, F. Ibrahim, A. Kerek, A. Krasznahorkay, M. Lewitowicz, S. Leenhardt, S. Lukyanov, P. Mayet, S. Mandal, H. van der Marel, W. Mittig, J. Mrázek, F. Negoita, F. De Oliveira-Santos, Zs. Podolyák, F. Pougheon, M. G. Porquet, P. Roussel-Chomaz, H. Savajols, Y. Sobolev, C. Stodel, J. Timár, and A. Yamamoto, Phys. Rev. C **69**, 034312 (2004).

[13] E. Becheva, Y. Blumenfeld, E. Khan, D. Beaumel, J. M. Daugas, F. Delaunay, Ch-E. Demonchy, A. Drouart, M. Fallot, A. Gillibert, L. Giot, M. Grasso, N. Keeley, K. W. Kemper, D. T. Khoa, V. Lapoux, V. Lima, A. Musumarra, L. Nalpas, E. C. Pollacco, O. Roig, P. Roussel-Chomaz, J. E. Sauvestre, J. A. Scarpaci, F. Skaza, and H. S. Than Phys. Rev. Lett. **96**, 012501 (2006).

[14] T. Aumann, Nucl. Phys. **A752**, 289c (2005).

[15] E. Sauran, F. Carstoiu, N. A. Orr, J. S. Winfield, M. Freer, J. C. Angélique, W. N. Catford, N. M. Clarke, N. Curtis, S. Grévy, C. Le Brun, M. Lewitowicz, E. Liégard, F. M. Marqués, M. Mac Cormick, P. Roussel-Chomaz, M.-G. Saint Laurent, and M. Shawcross, Phys. Rev. C **69**, 044603 (2001).

[16] R. Palit, P. Adrich, T. Aumann, K. Boretzky, D. Cortina, U. Datta Pramanik, Th.W. Elze, H. Emling, M. Fallot, H. Geissel, M. Hellström, K. L. Jones, L. H. Khiem, J. V. Kratz, R. Kulessa, Y. Leifels, A. Leistenschneider, G. Münzenberg, C. Nociforo, P. Reiter, H. Simon, K. Sümmerer and W. Walus, Nucl. Phys. **A731**, 235 (2004).

[17] D. Cortina-Gil, J. Fernandez-Vazquez, T. Aumann, T. Baumann, J. Benlliure, M. J. G. Borge, L. V. Chulkov, U. Datta Pramanik, C. Forssén, L. M. Fraile, H. Geissel, J. Gerl, F. Hammache, K. Itahashi, R. Janik, B. Jonson, S. Mandal, K. Markenroth, M. Meister, M. Mocko, G. Münzenberg, T. Ohtsubo, A. Ozawa, Y. Prezado, V. Pribora, K. Riisager, H. Scheit, R. Schneider, G. Schrieder, H. Simon, B. Sitar, A. Stolz, P. Strmen, K. Sümmerer, I. Szarka, and H. Weick, Phys. Rev. Lett. **93**, 062501 (2004).

[18] M. Stanoiu, F. Azaiez, Zs. Dombrádi, O. Sorlin, B. A. Brown, M. Belleguic, D. Sohler, M. G. Saint Laurent, Y.E. Penionzhkevich, G. Sletten, C. Borcea, C. Bourgeois, A. Bracco, J. M. Daugasd, Z. Dlouhý, C. Donzaud, Zs. Fül öp, D. Guillemaud-Mueller, S. Gr évy, F. Ibrahim, A. Kerek, A. Krasznahorkay, M. Lewitowicz, S. Lukyanov, P. Mayet, S. Mandal, W. Mittig, J. Mrázeki, F. Negoita, F. De Oliveira-Santos, Zs. Podolyák, F. Pougheon, P. Roussel-Chomaz, H. Savajols, Y. Sobolev, C. Stodel, J. Timár and A. Yamamoto, Nucl. Phys. **A746**, 135c (2004).

[19] E. Khan and Nguyen Van Giai, Phys. Lett. **B472**, 253 (2000).

[20] E. Khan, Y. Blumenfeld, Nguyen Van Giai, T. Suomijärvi, N. Alamanos, F. Auger, G. Colò, N. Frascaria, A. Gillibert, T. Glasmacher, M. Godwin, K. W. Kemper, V. Lapoux, I. Lhenry, F. Maréchal, D. J. Morrissey, A. Musumarra, N. A. Orr, S. Ottini-Hustache, P. Piattelli, E. C. Pollacco, P. Roussel-Chomaz, J. C. Roynette, D. Santonocito, J. E. Sauvestre, J. A. Scarpaci and C. Volpe, Phys. Lett. **B490**, 45 (2000).

[21] E. Khan, N. Sandulescu, M. Grasso, and Nguyen Van

Giai, Phys. Rev. C **66**, 024309 (2002).
[22] G. Giambrone, S. Scheit, F. Barranco, P. F. Bortignon, G. Colò, D. Sarchi and E. Vigezzi, Nucl. Phys. **A726**, 3 (2003).
[23] A. Obertelli, S. Péru, J. -P. Delaroche, A. Gillibert, M. Girod, and H. Goutte, Phys. Rev. C **71**, 024304 (2005).
[24] D. Vretenar, A. V. Afanasjev, G. A. Lalazissis and P. Ring, Phys. Rep. **409**, 101 (2005).
[25] Y. Utsuno, T. Otsuka, T. Mizusaki, and M. Honma, Phys. Rev. C **60**, 054315 (1999).
[26] B. A. Brown, P. G. Hansen, and J. A. Tostevin, Phys. Rev. Lett. **90**, 159201 (2003).
[27] A. Volya and V. Zelevinsky, Phys. Rev. Lett. **94**, 052501 (2005).
[28] A. Valor, P.-H. Heenen and P. Bonche, Nucl. Phys. **A671**, 145 (2000).
[29] M. Bender, P. Bonche, T. Duguet, and P.-H. Heenen, Phys. Rev. C **69**, 064303 (2004).
[30] M. Bender and P.-H. Heenen, Eur. Phys. J. A 25, s01, 519 (2005).
[31] B. Gall, P. Bonche, J. Dobaczewski, H. Flocard, and P.-H. Heenen, Z. Phys. **A348**, 183 (1994).
[32] J. Terasaki, P.-H. Heenen, H. Flocard and P. Bonche, Nucl. Phys. **A600**, 271 (1996).
[33] E. Chabanat, P. Bonche, P. Haensel, J. Meyer and R. Schaeffer. Nucl. Phys. **A635**, 231 (1998); Nucl. Phys. **A643**, 441(E) (1998).
[34] M. Bender, H. Flocard and P.-H. Heenen, Phys. Rev. C **68**, 044321 (2003).
[35] M. Bender and P.-H. Heenen, Nucl. Phys. **A713**, 39 (2003).
[36] K. Rutz, J. A. Maruhn, P.-G. Reinhard, and W. Greiner, Nucl. Phys. **A590**, 680 (1995).
[37] P. Bonche, J. Dobaczewski, H. Flocard, P.-H. Heenen and J. Meyer, Nucl. Phys. **A510**, 466 (1990).
[38] B. Sabbey, M. Bender, G. Bertsch and P.-H. Heenen, submitted to Phys. Rev. C, nucl-th/0611089.